Synthetic Protein Targeting by the Intrinsic Biorecognition Functionality of Poly(ethylene glycol) Using PEG Antibodies as Biohybrid Molecular Adaptors

Janne T. Hyotyla,[†] **Jie Deng,**[‡] **and Roderick Y. H. Lim**[†,*]

[†]Biozentrum and the Swiss Nanoscience Institute, University of Basel, Klingelbergstrasse 70, Basel 4056, Switzerland and [‡]Institute of Materials Research and Engineering, A*STAR (Agency for Science, Technology and Research), 3 Research Link, Singapore 117602

Considerable efforts are being made in biomaterials and biointerface science to engineer biocompatible materials that exhibit recognition and specificity.[1−5] According to Elbert and Hubbell,[2] this refers to the ability to "endow an entirely synthetic material with the biological recognition characteristics of biological macromolecules". Lying at the intersection between biology and materials science, biorecognition materials not only are important for exerting control over biological processes (*e.g.*, tissue regeneration)[6] but are envisaged to impart bioinspired functionality in technological systems.[1,3]

An area that is of important practical benefit lies in how biorecognition materials can regulate molecular sorting and precision immobilization in complex biological fluids.[1,2,5,7] To put this in perspective, the way specific proteins are sorted and delivered to exact spatial locations (*e.g.*, organelles) within the complex environment of the cell (*i.e.*, protein targeting)[8] is physically unprecedented. One problem lies with protein denaturation on engineered surfaces[9] that often leads to nonspecific contamination and fouling. For instance, protein microarrays where surface-immobilized proteins capture analyte molecules from solution are known to suffer from these effects.[7,10] This can be remedied by constructing biocompatible polymer brushes chemically derivatized with biotin,[11,12] or histidine-binding nitrilotriacetate (NTA)−metal ion complexes,[13] to impart both antifouling and biorecognition properties at biointerfaces. These then allow for the binding of streptavidin-modified or His-tagged proteins,

ABSTRACT Biointerfaces capable of biological recognition and specificity are sought after for conferring bioinspired functionality onto synthetic biomaterials systems. This is important for biosensing, bioseparations, and biomedical materials. Here, we demonstrate how intrinsic polymer−protein interactions between highly localized polyethylene glycol (PEG) brushes and PEG-binding antibodies can be used for sorting specific biomolecules from complex bulk biological fluids to synthetic nanoscale targets. A principal feature lies with the antifouling property of PEG that prevents unspecific binding. Exclusive access is provided by anti-PEG, which acts as a biohybrid molecular adaptor that sifts out and targets specific IgG "cargo" from solution to the PEG. The PEG can be reversibly washed and targeted in blood serum, which suggests potential benefits in technological applications. Moreover, anti-PEG binding triggers a stimuli-responsive conformational collapse in the PEG brush, thereby imparting an intrinsic "smart" biorecognition functionality to the PEG that can considerably impact its use as an antifouling biomaterial.

KEYWORDS: biointerface · biomimetics · biomaterials · biosensing · protein microarray · PEGylation · polymer brush · antibody · protein targeting · nuclear pore complex

respectively. While successful, it should be noted that these chemical-based strategies impart a property of *extrinsic* biorecognition (*i.e.*, indirect) because the proteins do not *a priori* recognize the polymers themselves. This imposes the limitation where only a predetermined set of tagged proteins can be targeted and not endogenous proteins sourced from authentic biological fluids. The latter aspect might be possible with proteins that are covalently immobilized on polymer brushes;[14] however no (extrinsic) biorecognition has yet been reported.

The objective of this work lies in exploiting the *intrinsic* protein−polymer biorecognition interactions between PEG-binding antibodies and PEG to sift out and sort specific molecular "cargoes" from a complex biological environment to site-specific targets.
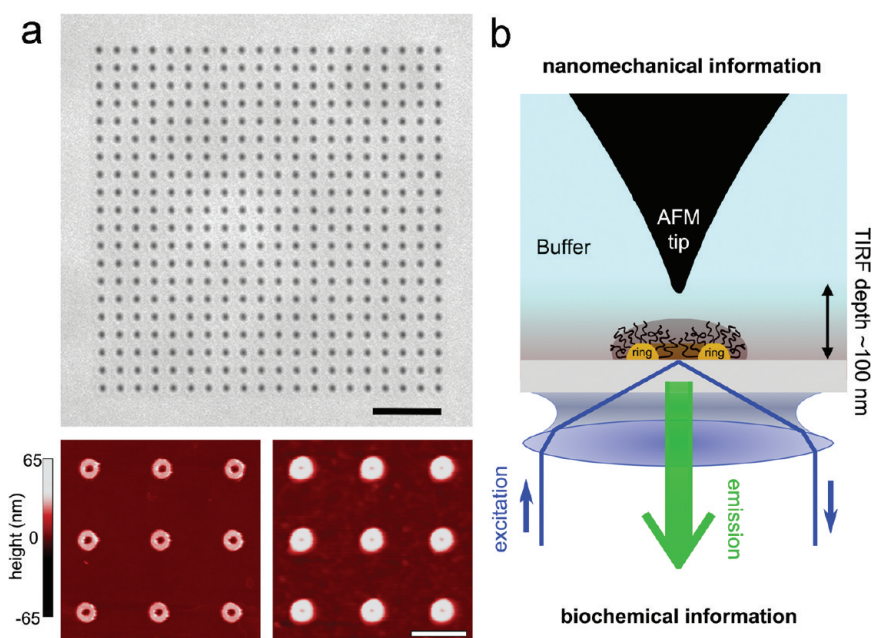
Figure 1. Combining nanofabrication, AFM, and TIRF. (a) Bright-field optical view of a 20 × 20 array of Au nanorings fabricated on a glass slide. Scale bar, 5 μm. Lower left: Individual nanorings resolved by AFM before PEGylation. Each nanoring is 1.3 μm apart from the next and exhibits a thickness and inner diameter and outer diameter of 27.1 ± 1.6 nm, 115 ± 8 nm, and 367 ± 6 nm, respectively. Lower right: A polymer brush barrier forms over each nanoring after PEGylation. Scale bar, 1 μm. (b) Combining AFM and TIRF allows for the direct correlation of local nanomechanical effects in the PEG brush to antibody-associated biochemical interactions occurring at each nanoring.

On the basis of its renowned properties of biocompatibility and protein resistance, PEG[15] is used extensively (i) in technology to impart fouling resistance against protein and cell adsorption on surfaces[16] and ultrafiltration membranes for water purification,[17] as well as (ii) in biomedical applications[18] to reduce immunogenicity and increase resistance to proteolytic cleavage in drug targeting.[15,18] Subsequently, PEG-binding antibodies have been developed for the identification and analysis of pharmacokinetic parameters of PEGylated molecules in drug development and clinical applications.[19−21] Nevertheless, it should be noted that the use of PEG-binding antibodies in the current context lies not in detecting PEGylated surfaces *per se*, but as biohybrid molecular adaptors or "receptors" that deliver and mediate the binding of specific protein "cargoes" to PEG. Further appeal rests in how intrinsic biorecognition interactions may exert a biomimetic stimuli-induced conformational change in the PEG. This so-called smart "protein-like" functionality is unique in comparison to current stimuli-responsive polymers where conformational changes are triggered by changes in solvent quality, pH, and temperature.[22]

RESULTS

To show how PEG-binding antibodies can be applied toward synthetic protein targeting, we obtained a PEG-binding mouse IgG monoclonal antibody (*i.e.*, E11;[19] henceforth known as anti-PEG) that is known to recognize the repeat ethylene oxide (EO) subunits on the PEG backbone. Immunoblot assays show that anti-PEG binds with high specificity to the 20 kDa PEG chains (Supporting Figure S1a). Its equilibrium dissociation constant is $K_D = 0.40 \pm 0.09$ nM, as measured by surface plasmon resonance (for details see Supporting Information and Figure S1b). Therefore, from a strict materials perspective, anti-PEG is remarkable in that it provides an exclusive biochemical interface for binding to PEG. To be precise, this is to our knowledge the first ever instance where a protein specifically recognizes and binds a completely synthetic, unmodified polymer (*i.e.*, the anti-PEG specifically recognizes the PEG backbone itself). Thereafter, we hypothesized that the anti-PEG could act as a biohybrid molecular adaptor that selectively targets specific secondary antibodies out of bulk solution and used (i) polyclonal donkey anti-mouse secondary IgG as model cargo ("specific IgG") and (ii) polyclonal donkey anti-rabbit secondary IgG ("unspecific IgG"), which does not bind anti-PEG as a fouling control.

Spatially distinct PEG targets were constructed by tethering 20 kDa methoxy-terminated polyethylene glycol (mPEG-SH) chains *via* covalent thiol bonds to Au nanorings ("PEGylated nanoring") (Figure 1a). The nanorings were fabricated 1.3 μm apart on glass slides in a 20 × 20 array format with each bare nanoring having a thickness and inner and outer diameter of 27.1 ± 1.6 nm, 115 ± 8 nm, and 367 ± 6 nm, respectively. A combined atomic force microscope (AFM) and total
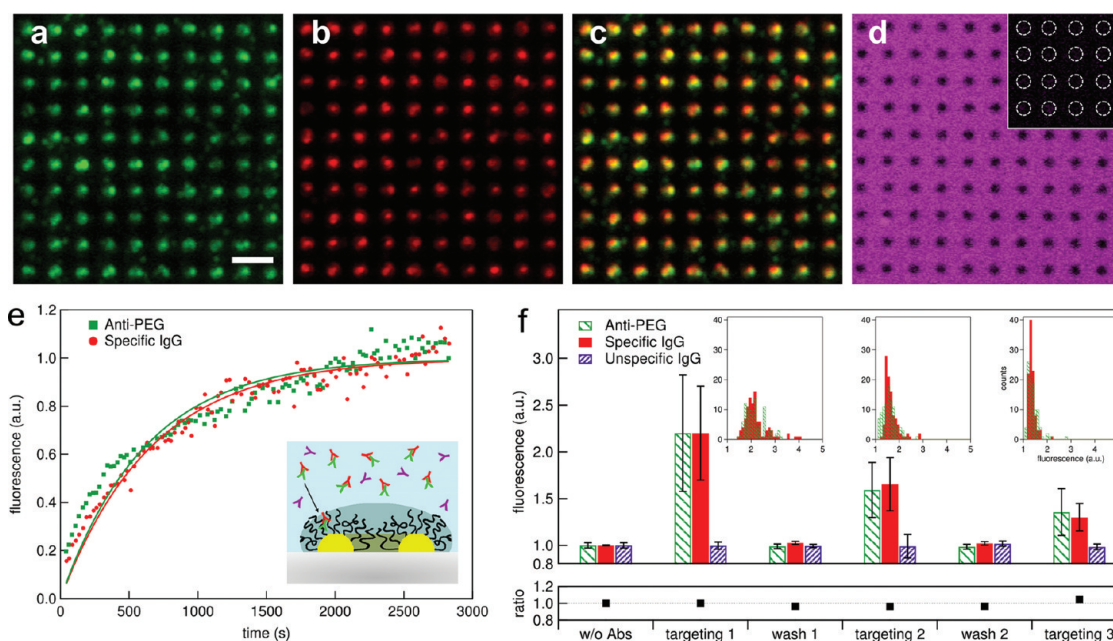
Figure 2. Precision targeting of specific IgG via anti-PEG. (a) TIRF reveals anti-PEG binding to each PEGylated nanoring. Scale bar, 2 μm. (b) The targeting of specific IgG from solution is marked and does not occur in the absence of anti-PEG (Figure 5). (c) Both signals show a clear co-localization when merged. (d) The "inverted contrast" in epifluorescence shows that nonspecific IgG is abundant in solution but does not accumulate at the PEGylated nanorings. This is confirmed by a lack of fluorescence in TIRF (inset). Dashed circles indicate the positions of individual nanorings. (e) The observed accumulation rates by time-lapse TIRF measurements are 1.6×10^{-3} and 1.5×10^{-3} s^{-1} for anti-PEG (green) and specific IgG (red), respectively. This indicates that specific IgG is being targeted to the PEGylated nanorings with anti-PEG. (f) Fluorescence quantification over consecutive targeting—wash cycles. By definition, the fluorescence intensity obtained in the absence of all three antibodies is set to unity. The mean nanoring intensities that remain at a constant 1:1 ratio (anti-PEG:specific IgG) indicate that targeting is reversible, as validated by the overlap in their intensity distributions (inset). The signal obtained for unspecific IgG does not change. Deviations from the mean intensity (denoted by error bars) indicate that differing numbers of anti-PEG and specific IgG molecules accumulate at each PEGylated nanoring.

internal reflection fluorescence (TIRF) microscope was used to correlate nanomechanical changes in the PEG chains to subsequent biochemical interactions *via* fluorescence, respectively (Figure 1b). After PEGylation, the hydrated PEG chains form polymer brushes, which act as barriers over individual nanorings.[23]

Figure 2 shows TIRF images obtained in a phosphate-buffered saline (PBS) solution simultaneously preincubated with Alexa488-labeled anti-PEG, Cy3-labeled specific IgG, Cy5-labeled unspecific IgG ($\sim$7 nM per antibody), and 1% (150 μM) unlabeled bovine serum albumin (BSA). Strong fluorescent signals corresponding to anti-PEG and specific IgG are seen at the PEGylated nanorings (Figure 2a to c). In comparison, inverted contrast is observed for unspecific IgG in epifluorescence (*i.e.*, the PEGylated nanorings are dark compared to the surrounding area), indicating a lack of localization despite being abundant in solution (Figure 2d). We note that this is also observed for specific IgG in the absence of anti-PEG (see later, Figure 5b). Time-lapse measurements recorded approximately equal accumulation rates of 1.6×10^{-3} and 1.5×10^{-3} s^{-1} for anti-PEG and specific IgG, respectively (Figure 2e), indicating that specific IgG is being escorted with anti-PEG from solution. This is

further supported by their mean fluorescence intensities and intensity distributions that are closely correlated over three consecutive targeting—washing cycles (Figure 2f; see Methods). The observed decrease in the net fluorescence intensity per cycle, however, may be attributed to the harsh 500 mM NaOH (pH 13.7) cleaning solution used to ensure complete removal of the antibodies during each washing step. This was later avoided by lowering the concentration and pH of the NaOH solution (see Figure 4b).

AFM force volume (FV) spectroscopy[23] was used to monitor changes in the PEG brush height under the influence of the different antibodies (Figure 3). In PBS, the PEG barrier height is 29.5 ± 4.8 and 34.2 ± 11.2 nm above the nanoring surface and the glass surface (at the nanoring center or "pore"), respectively. After adding the specific and unspecific IgGs, the barrier height at these locations reduces to 24.4 ± 1.6 and 29.5 ± 9.0 nm, respectively. This reduction in PEG height could arise from physical interactions (*e.g.*, van der Waals force) occurring between the non-PEG-binding antibodies and the underlying gold surface that would exert a "compressive" effect on the intervening PEG brush.[24] Nevertheless, their lack of accumulation (as seen in TIRF; see Figure 5) suggests that the PEG is still
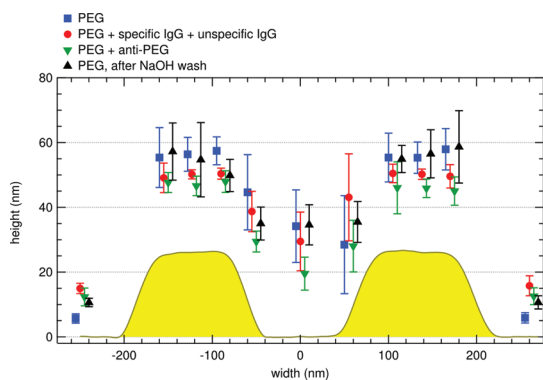
Figure 3. Correlating nonbinding/binding interactions to conformational changes in the PEG barrier. The PEG brush forms a barrier in PBS that envelops the nanoring surface and the central pore, respectively. A slight reduction at both the nanoring and the pore is measured in the presence of specific and unspecific IgGs. Anti-PEG binding elicits a strong reduction that is more obvious at the pore because the PEG chains collapse to their tethering sites along the inner wall (not to the pore's basal glass surface). After removal of anti-PEG with NaOH, the brush height re-extends to its original brush height. The outermost measurements (*i. e.*, < −200 nm and >200 nm) result from the adsorption of BSA and/or nonspecific molecules to the glass surface surrounding the nanorings. Force curves acquired at the outer nanoring edge have been omitted due to unstable tip contact. The average cross-section of a bare nanoring is shown (yellow). Error bars denote the standard deviation at each point.

in a brush-like barrier state. When anti-PEG is bound to the PEG (as confirmed by TIRF), the height at the nanoring surface and the pore further reduces to 20.0 ± 2.8 and 19.5 ± 5.1 nm, respectively. Closer inspection reveals dominant tip instabilities in individual force curves, signifying that the PEG brush barrier is disrupted by anti-PEG binding (Supporting Figure S2). Subsequently, the PEG brush barrier recovers to a height of 29.6 ± 8.0 nm (nanoring) and 34.6 ± 6.2 nm (pore) after removing the anti-PEG using NaOH. This reversible "collapse" of the PEG chains might explain how the brush can maintain its antifouling property over several targeting–wash cycles.

Finally, all three antibodies (∼7 nM per antibody) were incubated in blood serum (containing 50–100 mg/mL protein and ∼2 mg/mL lipids) to assess the effectiveness and reversibility of our synthetic protein targeting assay in an authentic, multicomponent biological fluid. As in PBS, the co-localization of specific IgG and anti-PEG is unmistakable (Figure 4a), with their ratios (anti-PEG:specific IgG) remaining close to unity over two consecutive NaOH wash–antibody incubation cycles (Figure 4b). Here, the 10 mM NaOH (pH 12) washing solution did not result in a decrease of the fluorescence intensity between cycles (compare with Figure 2f). Hence, PEG not only is antifouling against nonspecific entities within the serum but also maintains its viability to anti-PEG binding (and specific IgG targeting) over consecutive washes. This shows that
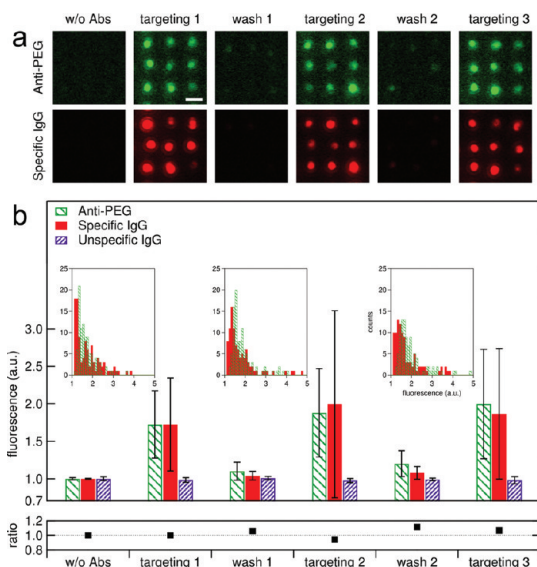

Figure 4. Reversible targeting in blood serum. (a) TIRF images obtained over three consecutive targeting–wash cycles. Anti-PEG successfully sifts out and targets specific IgG from serum to the PEGylated nanorings. Targeting is reversible after two 10 mM NaOH washing steps, although the number (intensity) of anti-PEG and specific IgG molecules can differ between PEGylated nanorings. Scale bar, 1 μm. (b) Fluorescence quantification at the PEGylated nanorings. By definition, the fluorescence intensity obtained in the absence of all three antibodies is set to unity. The overall intensities of specific IgG and anti-PEG are reproducible over two targeting–wash cycles with an approximate 1:1 distribution ratio (inset). Accumulation of the unspecific IgG does not occur at the PEGylated nanorings. The error bars denote deviations from the mean intensity.

specific IgG targeting by anti-PEG is robust, reproducible, and reversible.

DISCUSSION

On the basis of these results, the use of the PEG–anti-PEG system may be able to resolve several issues related to interfacial protein stability. First, PEG targets do not denature in complex biological environments (except oxidation by alcohol dehydrogenase).[25] Second, the mode of specific IgG capture by anti-PEG in solution before PEG targeting precludes binding artifacts and potential loss of bioactivity that result from the surface immobilization of capture proteins/antibodies (*e.g.,* from denaturing and molecular orientation effects).[7,10] Third, precision targeting from a complex milieu (*i.e.*, serum) is achieved without sample prepurification given the antifouling characteristics of PEG. Likewise, no washing steps or dilutions are required for targeting. Fourth, given its inability to denature, PEG targets can be reversibly washed and targeted unlike surface-bound protein targets. Fifth, PEG preserves and maintains antibody bioactivity on surfaces.[26] By incubating the antibodies sequentially, we find that specific IgG binds to anti-PEG prebound to the PEGylated nanorings but not to anti-PEG
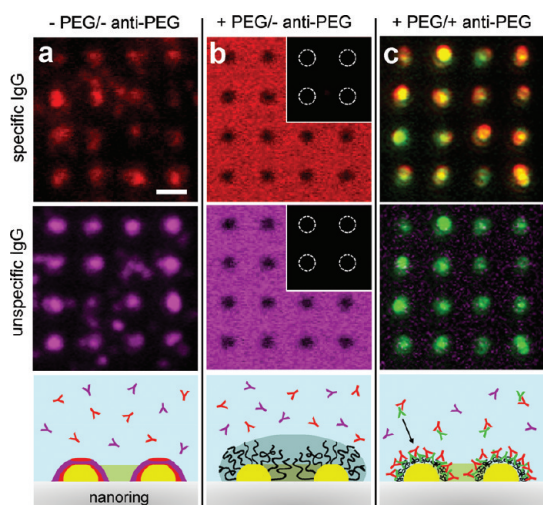
Figure 5. Molecular sorting, selective targeting, and surface fouling are interconnected effects. (a) Fouling: in the absence of PEG and anti-PEG, TIRF images show that "red", specific IgG (top) and "magenta", unspecific IgG (center) bind nonspecifically to (foul) the bare nanorings. (Bottom) Red Y's and magenta Y's correspond to specific IgG and unspecific IgG in solution, respectively. Fouling is denoted by the red and magenta bands over the nanoring. Scale bar, 1 μm. (b) Antifouling: in the absence of anti-PEG, the PEGylated nanorings remain dark in epifluorescence, although specific IgG (top) and unspecific IgG (center) are abundant in solution. The lack of fouling at the nanorings (TIRF, inset) indicates that both antibodies are being repelled by the PEG brush barrier (bottom). (c) Precision targeting: in the presence of "green" anti-PEG, specific IgG is distinctly co-localized with anti-PEG at the PEGylated nanorings (top). In contrast, unspecific IgG does not co-localize (center). By binding specifically to anti-PEG, specific IgG is precisely targeted to the PEGylated nanorings via exclusive anti-PEG binding interactions with the PEG (bottom). This is accompanied by a conformational compaction or "collapse" of the PEG brush.

nonspecifically adsorbed on the glass (Supporting Figure S3). Therefore, this method of preloading PEG with anti-PEG may be even applied in ELISA-based assays.[7] Sixth, the relative ease at which PEG functionalization can be carried out enhances the prospect of nanoscale miniaturization in biodiagnostics (i.e., a protein microarray spot size is typically ~200 μm, whereas our targets are submicrometer in size).[27] Altogether, these attributes satisfy six out of the eleven performance benchmarks listed by Wu et al. concerning the future development of assay capture surfaces in complex biological milieus.[7]

The biochemical selectivity and spatial targeting precision we observe is governed by applying a concept that accounts for molecular sorting, selective targeting, and surface fouling as closely interconnected effects. As we illustrate in Figure 5, this requires (1) a nanoscale target exhibiting antifouling properties in complex media (e.g., PEG brush); (2) a molecular adaptor with exclusive access to the intended target (e.g., anti-PEG); and (3) a suite of specific cargoes that do not themselves bind to the target but instead

"hitchhike" along with the molecular adaptor (e.g., specific IgG). Based on these hierarchical principles, its implementation is not likely limited to PEG-based systems alone. Nevertheless, PEG-based applications can benefit from expanding the repertoire of target cargoes by engineering bispecific antibodies[28] (or other antibody variants)[29] that would similarly act as biohybrid molecular adaptors that bind to PEG and another epitope (e.g., a disease biomarker). This adds a biochemical versatility that may be advantageous over the use of chemically derivatized biorecognition polymers[13] given the fact that untagged endogenous proteins can be sourced directly from authentic biological fluids. In combination with nonfouling PEGylated surfaces, such biohybrid adaptors could have potential applications spanning from nanopatterning to biosensing technologies and for regulating molecular transport processes more generally.

Technological implications aside, we observe that anti-PEG binding leads to a reduction in the repulsive Z-range of the PEG brush barrier that correlates to a conformational compaction. This might stem from a loss of conformational entropy in the PEG that is further exacerbated by the presence of several anti-PEGs that bind in a bivalent manner either intermolecularly between PEG chains or intramolecularly along a single chain. While theoretical efforts are starting to yield insight into the underlying physics of such behavior,[30] the relevance of this biomimetic effect, where intrinsic biorecognition and binding can induce conformational changes in an entirely synthetic polymer, resides in how it is analogous to the folding of intrinsically disordered (also called natively unfolded) proteins[31] upon binding to a ligand. This so-called "protein-like" functionality is unique in comparison to current stimuli-responsive polymers, where conformational changes are triggered by changes in solvent quality, pH, and temperature.[22] From a structural viewpoint, resolving exactly how anti-PEG binds to the PEG backbone may provide further insight into the molecular basis of fouling resistance in PEG.[32]

The essence of our work lies in being able to connect a biological material system to an abiological one by intrinsic biorecognition. Specifically, anti-PEG acts as a biohybrid molecular adaptor that can be used to sift specific proteins out of complex biological fluids for immobilization onto PEGylated targets. In part, this is inspired by how biological "adaptors" (known as transport receptors or karyopherins) identify and target specific proteins (deemed for transport into the nucleus) from the cytoplasm to nuclear pore complexes in eukaryotic cells.[33] In fact, the central pore of the nuclear pore complex is comprised of several intrinsically disordered proteins, which have been implicated in regulating the transport of selective cargo by reversibly collapsing during binding with karyopherins.[34] Thus, it may be possible to harness the binding-

induced collapse of PEG to function as a selective gating mechanism in stimuli-responsive nanoporous membranes[35] (as opposed to changing solvent conditions).[23]

METHODS

Au Nanoring Fabrication and Functionalization. Arrays of 20 × 20 Au nanorings were fabricated as described previously[23] on 0.17 ± 0.02 μm thick standard microscopy cover glass slides (round, 24 mm diameter; Karl Hecht Assistent, Germany) to allow for fluorescence imaging. The nanoring structures were designed with nominal inner and outer diameters of 80 and 400 nm and 1.3 μm pitch between rings. Sample cleaning was performed as described[23] followed by functionalization by immersing the nanoring arrays in 2 mM 20 kDa thiolated methoxy-polyethylene glycol (mPEG-SH, Laysan Bio, USA) dissolved in deionized H_2O (Milli-Q System, Millipore, USA) for 24 h at room temperature. Afterward, the samples were rinsed and ultrasonicated in deionized H_2O for 10 s and dried in a stream of N_2 gas. The samples were used immediately for measurements.

Antibodies. Monoclonal mouse IgG_1 antibodies against PEG (E11, anti-PEG)[19] were covalently labeled at the N-terminus with Alexa Fluor 488 5-SDP ester (A30052, Invitrogen, USA) for 2 h at room temperature with a 10× molar excess of dye according to the manufacturer's protocol. UV/vis spectrophotometry indicated a labeling efficiency of ∼1 dye molecule per antibody by comparing absorbance at 280 nm (protein) and 494 nm (dye) after purification of the labeled anti-PEG. Cy3-labeled polyclonal donkey anti-mouse (715-165-151, Jackson Immunoresearch, USA) and Cy5-labeled polyclonal donkey anti-rabbit (711-175-152, Jackson Immunoresearch) were used as the specific and unspecific IgG, respectively. UV/vis showed ∼1 dye molecule per antibody for both.

Solutions. Phosphate-buffered saline with 1.5 mM KH_2PO_4, 2.7 mM Na_2HPO_4, and 155.2 mM NaCl, pH 7.2, was obtained from Invitrogen (USA). Bovine serum albumin (10 mg/mL, fraction V; A9647, Sigma-Aldrich, USA) was dissolved in PBS to obtain a 1% BSA solution. Rabbit serum was obtained from Eurogentec (Belgium). A 5 μL amount of 1 M Tris-buffer, pH 8, was added per 100 μL of serum. NaOH solutions (10 and 500 mM) in deionized water (pH 12 and pH 13.7, respectively) were used as washing solutions for binding reversibility experiments (in Figures 4b and 2f, respectively).

Antibody Incubation. Anti-PEG, specific IgG, and/or unspecific IgG antibodies were preincubated together with either 1% BSA or rabbit serum at their final concentrations for at least 1 h prior to use. BSA was used in all PBS-based experiments to reduce the unspecific adsorption of antibodies (so as to reduce background fluorescence) on the glass substrate with the following exceptions: (i) AFM force measurements in the absence of antibodies (i.e., PBS; Figure 3), (ii) after NaOH washing (Figure 3), and (iii) the fouling control (Figure 5a). BSA was not used in the blood serum experiments given that rabbit serum albumin was already present. Solutions were pipetted on individual samples (preincubated for 15 min in 1% BSA or serum) and incubated for 30 min in darkness. Fluorescence and AFM measurements were performed without washing the sample or replacing/diluting the solution.

After the first incubation was performed as above, the reversibility data in PBS (Figure 2f) were obtained by applying 400 of 500 mM NaOH (pH 13.7) in deionized water to the sample surface for 30 min in darkness, after which the sample was rinsed with deionized water. This rather harsh condition affected the quantitative reversibility of anti-PEG binding over subsequent targeting–wash cycles (Figure 2f), but was important at the time to ensure the complete removal of prebound antibodies. Over the course of our later experiments in blood serum (Figure 4), we subsequently found that 10 mM NaOH (pH 12) was the optimal condition to clean and regenerate the PEG, all other aspects of the cleaning protocol remaining the same. Therefore, the extent of PEG regeneration can vary with NaOH conditions.

For time-lapse measurements, the sample surface was preincubated as above. Fluorescence images were taken before adding antibodies and directly after addition. For each time point, the sample surface was manually focused before taking an image.

Combined TIRF/AFM Setup. A combined total internal fluorescence microscope and atomic force microscope was used for all experiments. Fluorescence images were obtained with a 1.46 NA TIRF 100× oil immersion objective (Leica Microsystems, Germany) with an additional tube magnification of 1.6× in a Leica DMI6000 B inverted microscope fitted with a TIRF module (Leica AM TIRF MC) using three solid-state lasers with wavelengths of 488, 561, and 635 nm. Bandpass filter cubes were used to select the desired fluorescence channels: excitation at 490 ± 10 nm, emission at 525 ± 25 nm for Alexa Fluor 488; excitation at 560 ± 5 nm, emission at 610 ± 33 nm for Cy3; excitation at 635 ± 5 nm, emission at 720 ± 30 nm for Cy5. The sample was automatically illuminated at the correct angle to achieve an evanescent wave decay length of 90 nm in TIRF mode or wide-field laser illumination of the sample in epifluorescence mode. Images were taken with an EMCCD camera (C9100-02, Hamamatsu, Japan) in 14-bit mode with a resulting pixel size of 50 nm/pixel. Data sets used for the analysis of fluorescence intensity were collected under the same parameters and constant EM gain. In Figures 2a–d, 4a, and 5, the exposure times for Alexa488, Cy3, and Cy5 were set at 2 s, 600 ms, and 3 s with constant EM gain, respectively. In Figure 5c, the Cy3 channel was exposed for 300 ms.

AFM measurements were performed with a Bioscope 2 system running under a Nanoscope V controller (Veeco, USA) integrated with the TIRF microscope. Topographic images were obtained using tapping mode in air (for non-PEGylated samples) using RTESP (Veeco) cantilevers with a tip radius of 10 nm and contact mode in PBS (for PEGylated samples) with Biolever cantilevers (BL-RC150VB, Olympus, Japan; and OBL, Veeco). Brush height measurements were performed in force volume mode, with 32 × 32 force measurements (the distance between each pixel is 25 nm) over a random selection of rings on the glass slide. Force curves were obtained at 1 μm/s loading rate with a maximal force of 400 pN. Rectangular Si_3N_4 Biolever cantilevers with sharpened pyramidal tips were used. The spring constant was measured by thermal tune for each cantilever and was on average 0.010 ± 0.003 N/m. The representative tip radius was determined using four tips (3 used and 1 unused) by scanning electron microscopy (SEM) to be 11 ± 2 nm. That is, no significant difference in tip radius was found between unused and used cantilevers.

Fluorescence Data Analysis. Fluorescence images were rotated, cropped, and pseudocolored using ImageJ (http://rsb.info.nih.gov/ij/). Brightness and contrast values were adjusted for best visual clarity. For Figures 2a–d, 4a, and 5, automatic background subtraction was performed as provided by ImageJ (sliding paraboloid method, radius 100 pixels).

Quantitative fluorescence intensity analysis in Figures 2 and 4 was performed identically for each condition with custom macros in ImageJ. Nanorings (10 × 10) within the array were selected for intensity analysis. First, individual nanoring intensities were obtained by averaging over all pixels enclosed within a diameter of 16 pixels. Next, the background intensity was averaged over an area of 100 × 500 pixels outside the ring array. The mean fluorescence intensity was calculated by averaging over the 100 individual nanoring intensities and dividing by the background intensity. We found that the mean fluorescence intensities obtained in the absence of antibodies gave values above background. This was caused by small autofluorescence effects at the nanorings, which we measured to be 2% above the background for Alexa488 and Cy3 and 6% above the

background for Cy5. Nevertheless, we accounted for these effects by subtracting the nonzero values from all mean fluorescence intensities on a per channel basis.

Subsequently, the mean intensities from Alexa488 and Cy3 were scaled to have the same value at the first targeting measurement with the same scaling factor being applied to each respective fluorescence channel throughout all the targeting and washing steps. The calculated fluorescence intensities were additionally offset so that background (autofluorescence subtracted) equals unity. In this way, the relative intensities remained self-consistent and allowed comparisons to be made within individual experimental sets. Histograms were calculated from these relative intensities with a bin width of 0.1 fluorescence unit.

For time-lapse fluorescence analysis, a single average fluorescence intensity value was extracted for each time point and plotted against time after the start of the incubation. The intensity was obtained by averaging fluorescence intensities within a diameter of 16 pixels over 100 rings. Each kinetic trace was fitted with the equation $I(t) = A[1 - \exp(-k_{obs}t)]$, with $I(t)$ being the fluorescence intensity at time t, A being the equilibrium intensity at infinite time, and k_{obs} being the observed kinetic rate constant. Each trace was normalized by A.

AFM Data Analysis. Cross-sectional height profiles were extracted from AFM topographic images with Gwyddion (http://gwyddion.net) and averaged to obtain the height of the non-PEGylated nanorings. Lateral dimensions were obtained by SEM.

Approach force curves were extracted at selected points (*i.e.*, over glass, over the ring, over the pore) from force volume maps in Nanoscope and analyzed with custom scripts in IGOR Pro (Wavemetrics, USA). The raw force *vs* piezo-displacement curves were transformed to force *vs* tip−sample distance curves as previously published.[23] The brush height was determined by fitting a single-exponential curve to the steric repulsive region of the curve and defined from the detectable onset of repulsion (at which the value of the exponential fit equaled 1 pN) to the region where the force increases to infinity (tip−sample distance equals zero). Curves that could not be fit by an exponential equation were discarded (~20% of all analyzed curves).

Supporting Information Available: Figure S1, immunoblot and binding affinity measurements by surface plasmon resonance; Figure S2, representative force curves; and Figure S3, sequential binding by time-lapse TIRF. This material is available free of charge *via* the Internet at http://pubs.acs.org.

REFERENCES AND NOTES

1. Castner, D. G.; Ratner, B. D. Biomedical Surface Science: Foundations to Frontiers. *Surf. Sci.* **2002**, *500*, 28–60.
2. Elbert, D. L.; Hubbell, J. A. Surface Treatments of Polymers for Biocompatibility. *Annu. Rev. Mater. Sci.* **1996**, *26*, 365–394.
3. Granick, S.; Kumar, S. K.; Amis, E. J.; Antonietti, M.; Balazs, A. C.; Chakraborty, A. K.; Grest, G. S.; Hawker, C.; Janmey, P.; Kramer, E. J.; *et al.* Macromolecules at Surfaces: Research Challenges and Opportunities from Tribology to Biology. *J. Polym. Sci. Part B: Polym. Phys.* **2003**, *41*, 2755–2793.
4. Nel, A. E.; Madler, L.; Velegol, D.; Xia, T.; Hoek, E. M. V.; Somasundaran, P.; Klaessig, F.; Castranova, V.; Thompson, M. Understanding Biophysicochemical Interactions at the Nano-Bio Interface. *Nat. Mater.* **2009**, *8*, 543–557.
5. Ratner, B. D. The Engineering of Biomaterials Exhibiting Recognition and Specificity. *J. Mol. Recognit.* **1996**, *9*, 617–625.
6. Hench, L. L.; Polak, J. M. Third-Generation Biomedical Materials. *Science* **2002**, *295*, 1014–.
7. Wu, P.; Castner, D. G.; Grainger, D. W. Diagnostic Devices as Biomaterials: A Review of Nucleic Acid and Protein Microarray Surface Performance Issues. *J. Biomater. Sci., Polym. Ed.* **2008**, *19*, 725–753.
8. Blobel, G. Protein Targeting (Nobel lecture). *ChemBioChem* **2000**, *1*, 87–102.
9. Gray, J. J. The Interaction of Proteins with Solid Surfaces. *Curr. Opin. Struct. Biol.* **2004**, *14*, 110–115.
10. Mitchell, P. A Perspective on Protein Microarrays. *Nat. Biotechnol.* **2002**, *20*, 225–229.
11. Falconnet, D.; Pasqui, D.; Park, S.; Eckert, R.; Schift, H.; Gobrecht, J.; Barbucci, R.; Textor, M. A Novel Approach to Produce Protein Nanopatterns by Combining Nanoimprint Lithography and Molecular Self-Assembly. *Nano Lett.* **2004**, *4*, 1909–1914.
12. Ruiz-Taylor, L. A.; Martin, T. L.; Zaugg, F. G.; Witte, K.; Indermuhle, P.; Nock, S.; Wagner, P. Monolayers of Derivatized Poly(L-lysine)-Grafted Poly(ethylene glycol) on Metal Oxides as a Class of Biomolecular Interfaces. *Proc. Natl. Acad. Sci. U. S. A.* **2001**, *98*, 852–857.
13. Barbey, R.; Lavanant, L.; Paripovic, D.; Schuwer, N.; Sugnaux, C.; Tugulu, S.; Klok, H. A. Polymer Brushes via Surface-Initiated Controlled Radical Polymerization: Synthesis, Characterization, Properties, and Applications. *Chem. Rev.* **2009**, *109*, 5437–5527.
14. Tugulu, S.; Arnold, A.; Sielaff, I.; Johnsson, K.; Klok, H. A. Protein-Functionalized Polymer Brushes. *Biomacromolecules* **2005**, *6*, 1602–1607.
15. Harris, J. M., *Poly(ethylene Glycol) Chemistry: Biotechnical and Biomedical Applications*; Plenum Press: New York, 1992.
16. Dalsin, J. L.; Hu, B. H.; Lee, B. P.; Messersmith, P. B. Mussel Adhesive Protein Mimetic Polymers for the Preparation of Nonfouling Surfaces. *J. Am. Chem. Soc.* **2003**, *125*, 4253–4258.
17. Asatekin, A.; Kang, S.; Elimelech, M.; Mayes, A. M. Anti-Fouling Ultrafiltration Membranes Containing Polyacrylonitrile-Graft-Poly(ethylene Oxide) Comb Copolymer Additives. *J. Membr. Sci.* **2007**, *298*, 136–146.
18. Knop, K.; Hoogenboom, R.; Fischer, D.; Schubert, U. S. Poly(ethylene Glycol) in Drug Delivery: Pros and Cons as Well as Potential Alternatives. *Angew. Chem., Int. Ed.* **2010**, *49*, 6288–6308.
19. Cheng, T. L.; Cheng, C. M.; Chen, B. M.; Tsao, D. A.; Chuang, K. H.; Hsiao, S. W.; Lin, Y. H.; Roffler, S. R. Monoclonal Antibody-Based Quantitation of Poly(ethylene Glycol)-Derivatized Proteins, Liposomes, and Nanoparticles. *Bioconjugate Chem.* **2005**, *16*, 1225–1231.
20. Cheng, T. L.; Wu, P. Y.; Wu, M. F.; Chern, J. W.; Roffler, S. R. Accelerated Clearance of Polyethylene Glycol-Modified Proteins by Anti-Polyethylene Glycol IgM. *Bioconjugate Chem.* **1999**, *10*, 520–528.
21. Su, Y. C.; Chen, B. M.; Chuang, K. H.; Cheng, T. L.; Roffler, S. R. Sensitive Quantification of PEGylated Compounds by Second-Generation Anti-Poly(ethylene glycol) Monoclonal Antibodies. *Bioconjugate Chem.* **2010**, *21*, 1264–1270.
22. Gil, E. S.; Hudson, S. M. Stimuli-Responsive Polymers and their Bioconjugates. *Prog. Polym. Sci.* **2004**, *29*, 1173–1222.
23. Lim, R. Y. H.; Deng, J. Interaction Forces and Reversible Collapse of a Polymer Brush-Gated Nanopore. *ACS Nano* **2009**, *3*, 2911–2918.
24. Halperin, A. Polymer Brushes that Resist Adsorption of Model Proteins: Design Parameters. *Langmuir* **1999**, *15*, 2525–2533.
25. Herold, D. A.; Keil, K.; Bruns, D. E. Oxidation of Polyethylene Glycols by Alcohol-Dehydrogenase. *Biochem. Pharmacol.* **1989**, *38*, 73–76.
26. Yoshimoto, K.; Nishio, M.; Sugasawa, H.; Nagasaki, Y. Direct Observation of Adsorption-Induced Inactivation of Antibody Fragments Surrounded by Mixed-PEG Layer on a Gold Surface. *J. Am. Chem. Soc.* **2010**, *132*, 7982–7989.

27. Rosi, N. L.; Mirkin, C. A. Nanostructures in Biodiagnostics. *Chem. Rev.* **2005**, *105*, 1547–1562.

28. Pluckthun, A.; Pack, P. New Protein Engineering Approaches to Multivalent and Bispecific Antibody Fragments. *Immunotechnology* **1997**, *3*, 83–105.

29. Chan, A. C.; Carter, P. J. Therapeutic Antibodies for Auto-immunity and Inflammation. *Nat. Rev. Immunol.* **2010**, *10*, 301–316.

30. Halperin, A.; Kroger, M. Ternary Protein Adsorption onto Brushes: Strong versus Weak. *Langmuir* **2009**, *25*, 11621–11634.

31. Tompa, P. *Structure and Function of Intrinsically Disordered Proteins*; CRC Press: Boca Raton, 2010.

32. Morra, M. On the Molecular Basis of Fouling Resistance. *J. Biomater. Sci., Polym. Ed.* **2000**, *11*, 547–569.

33. Terry, L. J.; Shows, E. B.; Wente, S. R. Crossing the Nuclear Envelope: Hierarchical Regulation of Nucleocytoplasmic Transport. *Science* **2007**, *318*, 1412–1416.

34. Lim, R. Y. H.; Fahrenkrog, B.; Koser, J.; Schwarz-Herion, K.; Deng, J.; Aebi, U. Nanomechanical Basis of Selective Gating by the Nuclear Pore Complex. *Science* **2007**, *318*, 640–643.

35. Ulbricht, M. Advanced Functional Polymer Membranes. *Polymer* **2006**, *47*, 2217–2262.